


Le Song^{1,2}
 Liandong Yu^{1*}
 Di Li²
 Purva P. Jagdale²
 Xiangchun Xuan² 

¹School of Instrument Science and Opto-electronic Engineering, Hefei University of Technology, Hefei, P. R. China
²Department of Mechanical Engineering, Clemson University, Clemson, SC, USA

Received September 3, 2019
 Revised November 26, 2019
 Accepted November 26, 2019

Research Article

Elastic instabilities in the electroosmotic flow of non-Newtonian fluids through T-shaped microchannels

Electroosmotic flow (EOF) has been widely used to transport fluids and samples in micro- and nanofluidic channels for lab-on-a-chip applications. This essentially surface-driven plug-like flow is, however, sensitive to both the fluid and wall properties, of which any inhomogeneity may draw disturbances to the flow and even instabilities. Existing studies on EOF instabilities have been focused primarily upon Newtonian fluids though many of the chemical and biological solutions are actually non-Newtonian. We carry out a systematic experimental investigation of the fluid rheological effects on the elastic instability in the EOF of phosphate buffer-based polymer solutions through T-shaped microchannels. We find that electro-elastic instabilities can be induced in shear thinning polyacrylamide (PAA) and xanthan gum (XG) solutions if the applied direct current voltage is above a threshold value. However, no instabilities are observed in Newtonian or weakly shear thinning viscoelastic fluids including polyethylene oxide (PEO), polyvinylpyrrolidone (PVP), and hyaluronic acid (HA) solutions. We also perform a quantitative analysis of the wave parameters for the observed elasto-elastic instabilities.

Keywords:

Elasticity / Microfluidic / Polymer solution / Shear thinning / Viscoelastic fluid
 DOI 10.1002/elps.201900331



Additional supporting information may be found online in the Supporting Information section at the end of the article.

1 Introduction

Electroosmotic flow (EOF) is an electric field-driven fluid motion that has been widely used in microfluidics-based lab-on-a-chip devices to transport fluids and samples [1]. It is generated by an electric force acting upon the free charge density inside the electric double layer (EDL) that is formed naturally at a fluid-solid interface [2]. This essentially surface-driven fluid flow has a plug-like velocity profile with several advantages over the traditional pressure driven flow such as free of moving parts and reduced sample dispersion, etc. [3, 4]. It is, however, sensitive to both the surface (i.e., microchannel walls) and fluid properties, of which any inhomogeneity may draw disturbances to the flow and even

instabilities [5, 6]. The variation of wall property can be caused by non-uniform patterning [7, 8], field effect control [9, 10], or induced charge effect [11, 12]. The variation of fluid property may be a result of Joule heating effects [13, 14] or exist inherently at the interface of two different fluids [15, 16]. One important example of the latter situation is the electrically driven mixing of two or more fluids with dissimilar properties [17, 18]. Particularly, electrokinetic instabilities [19] have been reported to occur in co-flowing fluids with electric conductivity [20–27] and/or permittivity gradients [28, 29], where chaotic [30] or even turbulent [31] flows have been observed at small Reynolds numbers. However, existing studies on EOF instabilities have been focused primarily upon Newtonian fluids [27], despite that many of the real chemical and biological solutions are actually complex fluids with certain elastic and/or shear thinning characteristics [32, 33].

Thus far, there have been only a handful of studies concerning the instability induced in the EOF of non-Newtonian fluids. This so-called electro-elastic instability was first reported by Bryce and Freeman [34], who observed

Correspondence: Professor Xiangchun Xuan, Department of Mechanical Engineering, Clemson University, Clemson, SC 29634-0921, USA

E-mail: xcxuan@clemson.edu

Fax: +1-864-656-7299

Abbreviations: DC, direct current; EDL, electric double layer; HA, hyaluronic acid; PAA, polyacrylamide; PB, phosphate buffer; PEO, polyethylene oxide; XG, xanthan gum

*Additional corresponding author: Prof. Liandong Yu

E-mail: liandongyu@hfut.edu.cn

Color online: See the article online to view Figs. 1–8 in color.

extensional instabilities in the flow of both high and low molecular-weight polyacrylamide (PAA) solutions through a microchannel constriction. The critical direct current (DC) voltage to drive the flow instability in the high molecular-weight PAA solution was found to be over an order of magnitude higher than in the low molecular-weight one because of the significantly weaker elasticity effect in the latter. The same authors demonstrated in a later work [35] that such polymer stretching-induced electro-elastic instabilities did not really enhance the fluid mixing as compared to that in the stable flow of Newtonian fluids. In another study, Ko et al. [36] experimentally investigated the effects of fluid rheological properties on the EOF of xanthan gum (XG), polyvinylpyrrolidone (PVP), polyethylene oxide (PEO), and PAA solutions through a constriction microchannel. They observed electro-elastic instabilities in the XG and PAA solutions that are both strongly shear thinning fluids. In contrast, the fluid elasticity alone did not cause any noticeable flow instabilities in the PVP or PEO solution that each exhibits insignificant shear thinning effects. It was found to actually suppress the electro-elastic instability in the strongly shear thinning and strongly elastic PAA solution.

In addition, Afonso et al. [37] numerically simulated the elastic instability in the EOF of Upper-Convected Maxwell fluids through a planar cross-slot device. Their 2D model predicted a direct flow transition from a stable symmetric state to a time-dependent asymmetric state without crossing the steady asymmetric state. This prediction was later experimentally verified by Pimenta and Alves [38] using dilute and semi-dilute PAA solutions in both cross-slot and flow-focusing microdevices. The authors also carried out a numerical simulation based on the Oldroyd-B model, which revealed the fundamental role of the large stresses developed inside the EDL that couples with the streamline curvature around the geometric corners in the onset and dynamics of electro-elastic instabilities. Very recently, Song et al. [39] studied the electrokinetic instability in viscoelastic fluid flows with conductivity gradients through a T-shaped microchannel. They found that the addition of PEO polymer into a Newtonian fluid alters the threshold electric field as well as the speed and temporal frequency of the instability waves. They also developed a 3D numerical model that considered only the increased viscosity and conductivity along with the suppressed EOF of the PEO solution. Their model predictions compared favorably with the experimental data except at the highest PEO concentration, which was attributed by the authors to the neglected fluid elasticity effect in the model that increases with the PEO concentration.

We extend in this work the recent studies of Pimenta and Alves [38] and Song et al. [39] by carrying out a comprehensive experimental investigation of the fluid rheological effects on the elastic instability in the EOF of non-Newtonian fluids through T-shaped microchannels. We use six types of phosphate buffer (PB)-based aqueous solutions (including Newtonian, XG, PVP, hyaluronic acid (HA), PEO, and PAA solutions) that have distinct elasticity and shear thinning properties with the goal of examining their individual and

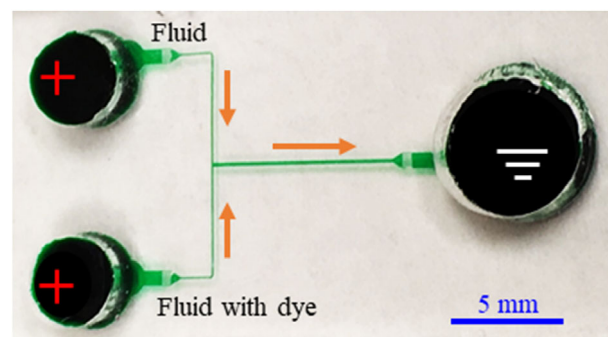


Figure 1. Top-view picture of the fabricated T-shaped microchannel. In the experiment the two inlet reservoirs were each imposed with an equal DC voltage (represented by a “+” symbol) and the outlet reservoir was grounded. The fluids supplied to the inlet reservoirs were identical except that one of them was mixed with fluorescently dye for visualizing the fluid interface. The block arrows indicate the flow directions.

combined effects on the electro-elastic instability. Conductivity gradients are minimized in any of these fluid flows to exclude the electrokinetic instability [19, 39]. We also use the PAA solution to further examine the effects of polymer concentration, buffer concentration and as well channel dimensions on electro-elastic instabilities. It is hoped that our work will stimulate more numerical and experimental studies on electro-elastic instabilities in relevant chemical and biological fluids for lab-on-a-chip applications.

2 Materials and methods

2.1 Microchannels

Symmetric T-shaped microchannels were used to study the elastic instability in the EOF of non-Newtonian fluids. They were fabricated with PDMS using the standard soft lithography technique. The detailed procedure was described in our earlier paper [40]. As shown in Fig. 1, each microchannel consists of a 10-mm long, 200- μm wide main-branch and two 8-mm long, 100- μm wide side-branches. It was made with three different depths, which were measured as 30, 50, and 67 μm , respectively. The (two) inlet and (one) outlet reservoirs were all made large with a 6-mm diameter each, which should help diminishing the influence of the EOF inside the microchannel on the liquid levels in the reservoirs. A freshly prepared microchannel was used in any test of a new fluid. It was primed with deionized water for at least 10 min to ensure the uniformity and reproducibility of surface properties (more specifically, the wall zeta potential).

2.2 Fluids

Six types of fluids with varying rheological properties were prepared in aqueous 1 mM PB solution (Thermo Fisher Scientific): (1) pure PB solution, Newtonian fluid; (2) 500 ppm

Table 1. Physical properties of the prepared solutions at room temperature. The elasticity number, El , was estimated based on the zero shear viscosity, η_0 , of the fluid because of the inherently weak EOF. The electroosmotic mobility, μ_{eo} , was experimentally measured. Other symbols include the fluid relaxation time, λ , and the power-law index, n

Solution	Polymer concentration	λ (ms)	η_0 (mPa·s)	n	El	μ_{eo} ($\times 10^{-8} \text{m}^2/\text{V} \cdot \text{s}$)
PB	0	0	1	1	0	3.8
XG ^{a)}	500 ppm	~0	19.7	0.58	~0	3.5
PVP ^{b)}	5%	2.2	28	~1	7.70	0.1
HA ^{c)}	1000 ppm	0.25	9.4	0.88	0.29	4.6
PEO ^{d)}	2000 ppm	2.6	4.5	0.93	1.46	0.1
PAA ^{e)}	200 ppm	95	22	0.38	261.2	4.2

^{a)}Japper-Jaafar et al. [41]; ^{b)}Liu et al. [42]; ^{c)}Lim et al. [43]; ^{d)}Rodd et al. [44]; ^{e)}Poole and Escudier [45].

XG solution (Tokyo Chemical Industry), negligibly elastic and strongly shear-thinning fluid [41]; (3) 5% PVP solution ($M_w = 360$ kDa, Sigma-Aldrich), strongly elastic and negligibly shear-thinning fluid [42]; (4) 1000 ppm HA solution ($M_w = 301 - 450$ kDa, Lifecore Biomedical), weakly elastic and weakly shear-thinning fluid [43]; (5) 2000 ppm PEO solution ($M_w = 2$ MDa, Sigma-Aldrich), mildly elastic and weakly shear-thinning fluid [44]; (6) 200 ppm PAA solution (molecular weight, $M_w = 18$ MDa, Polysciences), strongly elastic and strongly shear-thinning fluid [45]. The rheological properties of these fluids are summarized in Table 1, which were extracted from the literature due to the lack of measuring equipment in our lab. It is important to note that these displayed properties are merely illustrative of the fluid characteristics. To study the parametric effects on the electro-elastic instability in PAA solutions, we varied the PAA concentration in 1 mM PB from 10 to 1000 ppm. We also varied the PB concentration from 0 mM to 10 mM while the PAA concentration was fixed at 200 ppm.

The shear-thinning effect of the prepared solutions is characterized by the power-law index, n , in Table 1, where a smaller value indicates a greater shear thinning effect (note a fluid with $n < 0.65$ can be viewed as a strongly shear thinning fluid [46]). The elasticity effect of the prepared fluids is often characterized by the Weissenberg number [36–38],

$$Wi = \frac{2\lambda V}{w} \quad (1)$$

where λ is the fluid relaxation time, V is the average electroosmotic velocity in the main-branch of the microchannel, and w is the width of the main-branch. A larger value of Wi indicates a stronger elasticity effect, which may be a result of either an extended relaxation time or an increased fluid velocity. The inertial effect is characterized by the Reynolds number [47, 48],

$$Re = \frac{2\rho V w h}{\eta(w+h)} \quad (2)$$

where ρ is the fluid density, h is the microchannel height, and η is the fluid viscosity. The Reynolds number is on the order of 0.01 in the majority of our tests. The maximum Re occurred in the PAA solution in the deepest microchannel with

a value of nearly 0.1, which is comparable to that reported by Pimenta and Alves [38]. The ratio of the Weissenberg number to the Reynolds number gives the so-called elasticity number [36, 44],

$$El = \frac{Wi}{Re} = \frac{\lambda\eta(w+h)}{\rho w^2 h} \quad (3)$$

Different from the Weissenberg number, the dimensionless elasticity number becomes independent of the fluid kinematics. A larger value of El indicates a stronger elasticity effect and $El > 1$ indicates a dominant elasticity effect over the inertial effect. Because of the small shear rate in EOFs except inside the EDL that is on the order of 10 nm thick [1, 2], we used the zero-shear viscosity, η_0 (Table 1), to estimate the value of El in Eq. (3) for simplicity. We acknowledge that η_0 may be significantly different from that inside the EDL for strongly shear thinning fluids, the latter of which actually determines the electroosmotic velocity among other flow characteristics. Therefore, the calculated values of El in Table 1 may be only rough approximations of the real values.

2.3 Methods

The electroosmotic fluid flow through T-shaped microchannels was driven by DC voltages that were supplied with a high-voltage DC power supply (Glassman High Voltage). An equal amount of DC voltage (no more than 500 V unless otherwise stated to minimize both the polymer agglomeration [34, 38] and the fluid Joule heating effects [13, 14]) was imposed upon each of the two inlet reservoirs while the outlet reservoir was grounded. This yielded a (nearly) equal flow velocity for the fluids in the two side-branches, which were identical except that one of them was mixed with 50 μM Rhodamine B dye (Sigma-Aldrich) for visualization of the fluid interface (see Fig. 1). The liquid heights in the inlet and outlet reservoirs were carefully balanced prior to every test to minimize the influence of pressure-driven flow. The test was performed at least three times in each prepared fluid. The dynamic behavior of the fluid interface at the T-junction of the microchannel was visualized through an inverted fluorescent microscope (Nikon Eclipse TE2000U; Nikon Instruments) equipped with

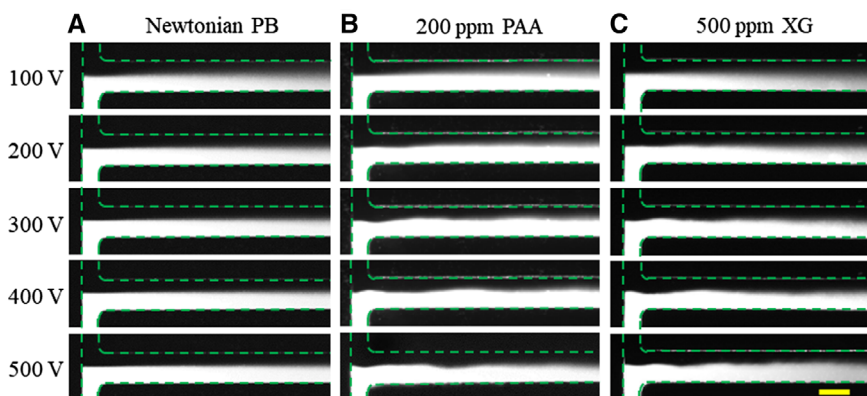


Figure 2. Experimental images (white for dyed solutions and dark for undyed solutions) for the EOF of 1 mM PB-based Newtonian solution (A), 200 ppm PAA solution (B), and 500 ppm XG solution (C) in a 50 μm deep microchannel under different DC voltages. The dashed lines on the images highlight the channel walls, and the scale bar represents 200 μm .

a CCD camera (Nikon DS-Qi1Mc). The recorded digital images and videos (at about 15 frames per second) were post-processed using the Nikon imaging software (NIS-Elements AR 2.30).

Fluid electric conductivity was measured using a conductivity meter (Accumet AP85, Fisher Scientific). No significant differences were observed in between the fluids with and without the dye (e.g., 178 and 183 $\mu\text{S}/\text{cm}$ for 1 mM PB solution without and with the dye, respectively). Therefore, the conductivity gradient-induced electrokinetic instability [19, 39] was not expected to take place in our tests. The electroosmotic mobility, μ_{EO} , of each of the prepared fluids was measured by tracking the front of neutral Rhodamine B dyes (Sigma Aldrich) with time (Table 1). Briefly, we measured the travel time of the dye front across the length of a straight rectangular microchannel that was made using the same protocol as the T-shaped one. The obtained electroosmotic velocity divided by the electric field then gave the value of the electroosmotic mobility in the test fluid.

3 Results and discussion

3.1 Fluid rheological effects on electro-elastic instabilities

To investigate the effect of fluid rheological properties on the elastic instability in EOFs, we performed tests with the prepared six types of 1 mM PB-based Newtonian and non-Newtonian solutions (Table 1) in a 50 μm deep microchannel. Figure 2 shows the top-view images for the flow of PB (1 mM), PAA (200 ppm) and XG (500 ppm) solutions, respectively, at the T-junction region of the microchannel under varying DC voltages. The fluid interface in the EOFs of Newtonian PB solution was found to remain stable (Fig. 2A) even under the DC voltage of up to 3000 V (data not shown). In contrast, wave-like flow disturbances were observed in both the PAA (Fig. 2B) and XG (Fig. 2C) solutions. These electro-elastic instabilities started occurring at the channel T-junction in both solutions when the applied DC voltage became higher than 200 V. They appeared to have relatively long wavelengths, but

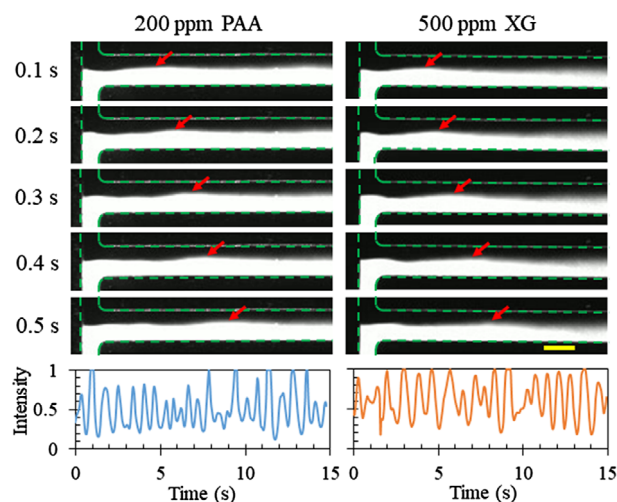


Figure 3. Sequences of images (top) and intensity plots of the fluid interface (bottom) in the EOF of 200 ppm PAA and 500 ppm XG solutions under a DC voltage of 400 V. The arrows on the images track the propagation of the electro-elastic instability waves. The dashed lines highlight the channel walls, and the scale bar represents 200 μm .

did not exhibit apparently periodic behaviors. To make this point clear, we obtained sequential images in the PAA and XG solutions, respectively, under the DC voltage of 400 V (Fig. 3, top). We also used the Nikon imaging software to track the intensity development of the fluid interface at the top of the T-junction in these images. As seen from the intensity plots in Fig. 3 (bottom), the fluid interfaces in both solutions oscillate with time. However, neither of them displays a single periodicity, which seems consistent with the recent observations from Pimenta and Alves [38] in the EOF of PAA solutions through a cross-slot geometry. As demonstrated by these authors [38], our obtained signals in Fig. 3 (bottom) may also be a sum of several harmonics mixed with some instrumentation noise.

We further did a quantitative analysis of the wave parameters for the observed elastic instabilities in the EOF of PAA and XG solutions under a range of DC voltages. The data

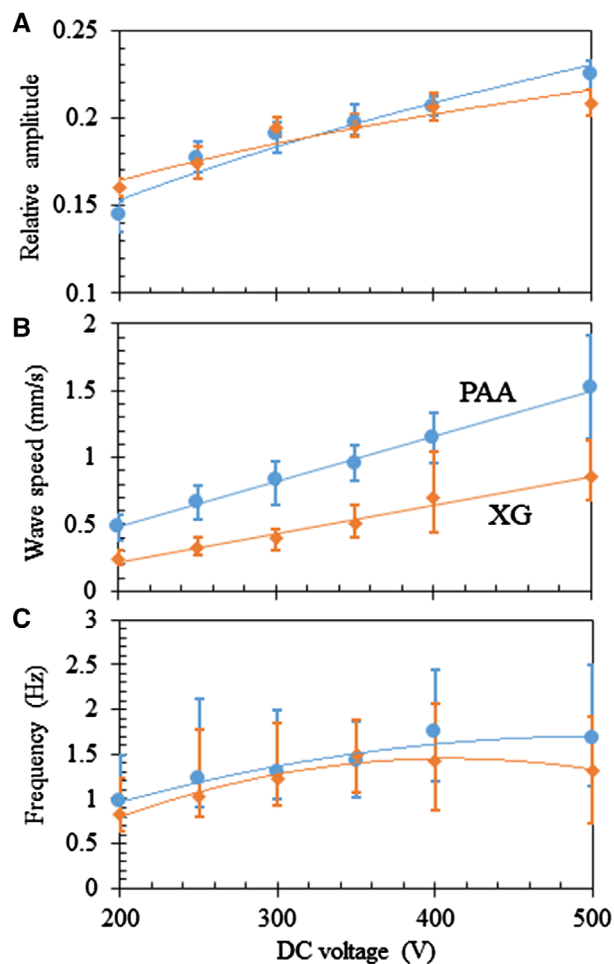


Figure 4. Quantitative plots of the experimentally measured wave parameters for the observed electro-elastic instabilities in 200 ppm PAA and 500 ppm XG solutions under a range of DC voltages: (A) Amplitude (relative to the width of the main-branch of the microchannel); (B) Speed; (C) Frequency. The curves represent the trendlines that are fitted to the experimental data points (symbols).

were obtained from at least 3 independent tests for each fluid. Figure 4A shows the wave amplitudes (relative to the width of the main-branch) in the two solutions, which both increase slowly with the increase of DC voltage. Moreover, they have comparable magnitudes under each electric field. Our observation in the PAA solution in Fig. 4A seems to be consistent with that reported by Pimenta and Alves [38], which was attributed to the increasing effect of fluid elasticity in terms of a greater Weissenberg number. Figure 4B shows the measured wave speeds in the PAA and XG solutions, which both increase with the DC voltage in an approximately linear relationship. This trend may imply the correlation of the wave speed with the EOF velocity that is proportional to the applied DC voltage via the electroosmotic mobility (Table 1). However, the wave speed in the PAA solution is slightly higher than the EOF velocity therein. In contrast, the wave speed in the XG solution is significantly lower than its EOF velocity. These

phenomena may be associated with the dissimilar elasticity effect between the two fluids and require further studies. Figure 4C shows the measured number of occurrences of the instability waves, which was obtained by simply counting the number of peaks in the intensity plot over the entire length of a 15 s video for each fluid and named as “frequency” here for easy references. The wave frequency in the PAA solution is slightly higher than in the XG solution. It is, however, much lower than that reported by Pimenta and Alves [38], the reason for which is currently unclear to the authors. In addition, the wave frequency plots in Fig. 4C each show a slowly increasing trend with the DC voltage of up to 400 V followed by a slight drop at 500 V. We did not test either solution under DC voltages of greater than 500 V because polymer gels were noticed in some of the tests in both solutions. It is noted that the formation of gels has been reported to occur in electric field-driven polymer flows in previous studies [34, 38].

Figure 5 shows the experimental images for the EOF of PVP (5%), PEO (2000 ppm) and HA (1000 ppm) solutions. No instability was noticed in any of these viscoelastic solutions under the DC voltage of up to 1000 V. Referring to the rheological properties of the prepared solutions in Table 1, we find that the electro-elastic instability may result primarily from the fluid shear-thinning effect. This is evident from the observations in PAA (Fig. 2B) and XG (Fig. 2C) solutions that are both strongly shear thinning. We speculate it might be because the shear thinning effect causes a significant variation of fluid viscosity at around both the geometry corners and the stagnation point of the T-junction region. This change may induce additional stresses coupled with the large stresses developed inside the EDL that has been recently verified by Pimenta and Alves [38] through numerical simulations. We are unable to judge if the fluid elasticity plays a significant role in the onset of electro-elastic instabilities because the PAA solution is strongly elastic with an elasticity number, $El = 261.2$ [49] while the XG solution is only weakly elastic with $El \sim 0$ [50]. We speculate that these two solutions may have similar microstructural effects (e.g., polymer-wall interaction and electric effect on the molecular structure of polymers, etc.) that can strongly influence the EOF. For example, the tendency of gelification in both solutions may be a possible explanation of our observations in Figs. 2 and 3.

3.2 Electro-elastic instabilities in PAA solutions

In this section, we choose PB-based PAA solutions for a further study of several other parametric effects on electro-elastic instabilities in T-shaped microchannels. We note that Pimenta and Alves [38] have recently performed a combined experimental and numerical investigation of the effects of DC voltage and polymer concentration on the elastic instability in the EOF of water-based PAA solutions through a cross-shaped microchannel. Both the flow-focusing and cross-slot configurations were tested in their work. However, the simulation performed by Pimenta and Alves [38] was based on the Oldroyd-B model that considers only the fluid elasticity effect

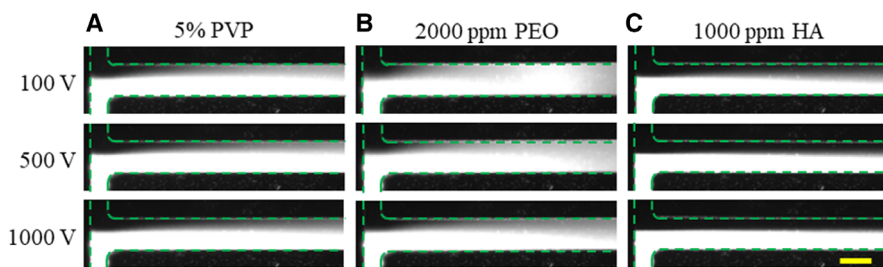


Figure 5. Experimental images (white for dyed solutions and dark for undyed solutions) for the EOF of 1 mM PB-based 5% PVP solution (A), 2000 ppm PEO solution (B), and 1000 ppm HA solution (C) in a 50 μm deep microchannel under different DC voltages. The dashed lines on the images highlight the channel walls. The scale bar represents 200 μm.

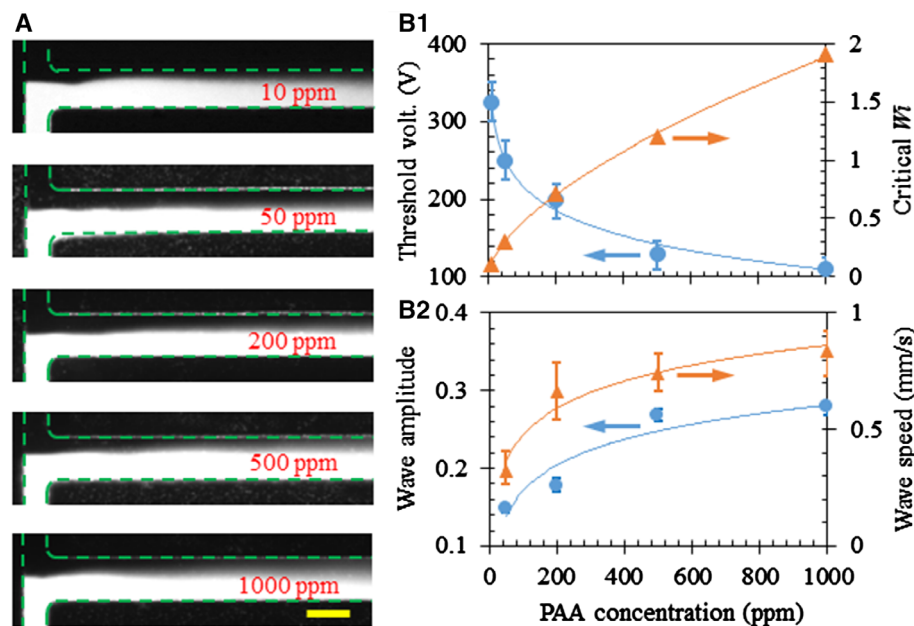


Figure 6. Effect of polymer concentration (labeled on the images) on the elastic instability in the EOF of 1 mM PB-based PAA solutions through a 50 μm deep microchannel: (A) shows the experimental images of the fluid interface at the T-junction under the threshold voltages; (B1) shows a graph for the measured threshold voltage and the corresponding calculated critical Weissenberg number, Wi_{cr} , using Eq. (4); (B2) shows a graph for the measured wave amplitude (relative to the width of the main-branch) and speed under 250 V DC. The curves in (B1) and (B2) represent the trendlines that are fitted to the experimental data points (symbols). The dashed lines on the images highlight the channel walls, and the scale bar represents 200 μm.

while neglecting the shear thinning effect. We will compare our experimental results on the polymer concentration effect in a T-shaped microchannel with theirs in a similar flow-focusing configuration if applicable. We will further study the effects of buffer concentration and channel dimensions on electro-elastic instabilities in T-shaped microchannels.

3.2.1 Effect of polymer concentration

We studied the effect of polymer concentration on the electro-elastic instability in 1 mM PB-based PAA solutions through a 50 μm deep microchannel. The DC voltage was increased with a step of 20 V in each test. However, once the fluid interface became visually unstable with the onset of wave-like structures, we switched to finely tune (up and/or down) the DC voltage in order to obtain the (minimum) threshold voltage. Figure 6A shows the images of the disturbed fluid interface in PAA solutions of varying concentrations under the corresponding threshold voltages. In 10 ppm PAA solution, intermittent wave-like instabilities started to occur at 325 V and we did not observe continuous waves at 500 V. In the solutions with 50 ppm and higher polymer concentrations, continuous wave-like disturbances appeared at the fluid inter-

face once the applied voltage reached the threshold value. We speculate this inversion may be related with the overlap concentration of the PAA solution, which was reported by Sousa et al. [51] to be around 45 ppm. However, there is no apparent change in the amplitude or frequency of the instability waves at the threshold voltage with the increase of the polymer concentration.

Figure 6B1 shows a graph of the experimentally measured threshold voltages. As the PAA concentration increases, the threshold voltage first decreases rapidly (for 200 ppm and lower) and then starts leveling off (for 500 ppm and higher). This trend seems consistent with that reported in the paper of Pimenta and Alves [38], where two concentrations of PAA solutions were tested. Figure 6B1 also shows the calculated value of the critical Weissenberg number, Wi_{cr} , at the measured threshold voltage, ϕ_{th} , for each PAA concentration,

$$Wi_{cr} = \frac{2\lambda E_{th}\mu_{EO}}{w} = \frac{2\lambda}{w} \frac{\phi_{th}}{L} \mu_{EO} \quad (4)$$

$$\lambda = \lambda_{200} \left(\frac{c}{c_{200}} \right)^{0.65} \quad (5)$$

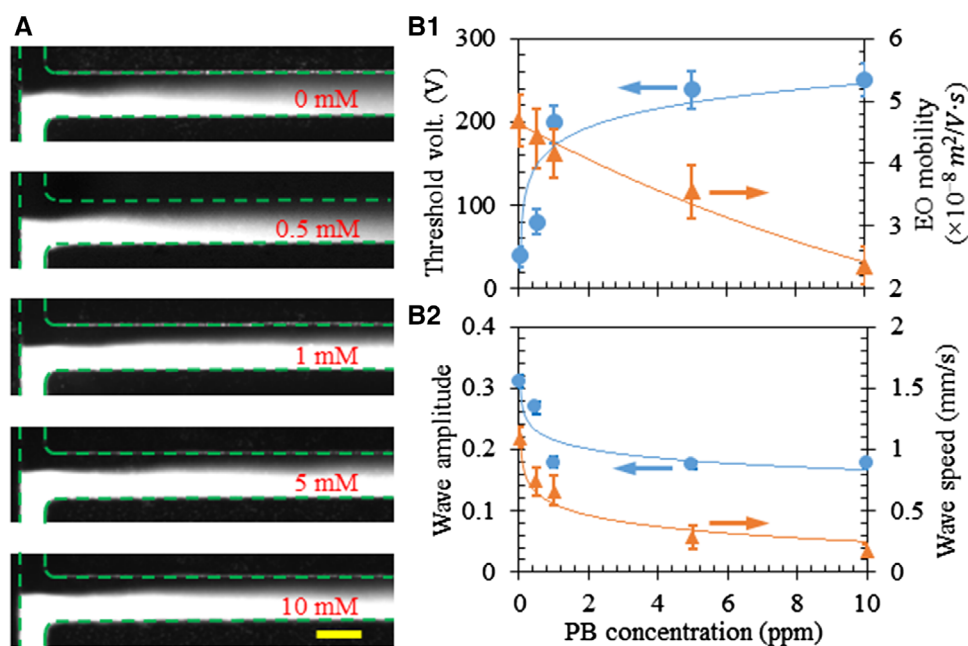


Figure 7. Effect of buffer concentration (labeled on the images) on the elastic instability in the EOF of PB-based 200 ppm PAA solutions through a 50 μm deep microchannel: (A) shows the experimental images of the fluid interface at the T-junction under the threshold voltages; (B1) shows a graph for the measured threshold voltage and electroosmotic mobility; (B2) shows a graph for the measured wave amplitude (relative to the width of the main-branch) and speed under 250 V DC. The curves in (B1) and (B2) represent the trendlines that are fitted to the experimental data points (symbols). The dashed lines on the images highlight the channel walls, and the scale bar represents 200 μm .

where $E_{th} = \phi_{th}/L$ is the threshold electric field with $L = 18 \text{ mm}$ being the total length of the side-branch and main-branch of the microchannel, μ_{EO} is the measured fluid electroosmotic mobility (see Supporting Information Figure S-1 for the mobility values in solutions of varying PAA concentrations), and the subscript “200” denotes a reference concentration of 200 ppm in our calculations. Note that Eq. (5) was obtained from the formula for the effective relaxation time [52], $\lambda = 18\lambda_{Zimm}(c/c^*)^{0.65}$, where λ_{Zimm} and $c^* = 45 \text{ ppm}$ [51] are the Zimm relaxation time and overlap concentration, respectively, and each a function of the polymer molecular weight. The critical Weissenberg number increases from 0.11 at 10 ppm to 1.90 at 1000 ppm, indicating an increasing effect of fluid elasticity. These values are comparable to those typically found in the pressure-driven flow of PAA solutions in cross-slot and flow-focusing configurations [51, 53]. They are, however, much larger than those reported for the EOF of PAA solutions in earlier studies (on the order of 0.01) [34, 38]. This discrepancy is at least partly because of the uncertainty of the fluid rheological properties (Table 1) used in our calculations. As the PAA solution also becomes increasingly shear thinning at a higher concentration, we are still unsure of which effect plays a dominant role. Figure 6B2 shows the measured amplitude and speed for electro-elastic instability waves in the PAA solution of varying concentrations. To compare the experimental data fairly, all measurements were performed under 250 V DC, at which the EOF becomes unstable in all PAA concentrations except 10 ppm (not included in the graph because of the lack of continuous waves; see Fig. 6A). Both wave parameters increase (first quickly and then leveling off) with the increase of the PAA concentration because of the enhanced instability in a more elastic and/or shear thinning fluid. The

measured frequency is found to remain approximately at 1 Hz in all PAA concentrations (see Supporting Information Figure S-2).

3.2.2 Effect of buffer concentration

The effect of buffer concentration on the electro-elastic instability was studied in PB-based 200-ppm PAA solutions through a 50 μm deep microchannel. Figure 7A shows the experimental images at the channel T-junction under the threshold voltages, where the PB concentration was varied from 0 (i.e., pure water-based, which is the background solution used in the paper of Pimenta and Alves [38]) to 10 mM. For all tested solutions, similar electro-elastic instabilities were observed to appear at the fluid interface. However, the measured threshold voltage exhibits a monotonically increasing trend with the increase of the buffer concentration. This trend, as shown by the line graph in Figure 7B1, is opposite to that of the threshold voltage when the polymer concentration increases (Figure 3B1). The threshold voltage climbs rapidly in the lower range of buffer concentrations (1 mM and lower) and levels off in the higher range (5 mM and above). The addition of salt has been reported to reduce both the shear-thinning and elasticity of PAA solutions [54]. We therefore speculate that increasing the buffer concentration of PAA solutions in our experiment further decreases these two rheological properties, which should be responsible for the observed increasing threshold voltage in Figure 7B1. Another factor may be the electroosmotic mobility that, as expected from the literature [55], was found in our experiment to decrease with the increase of PB concentration (Figure 7B1). This variation reduces the stresses developed inside the EDL

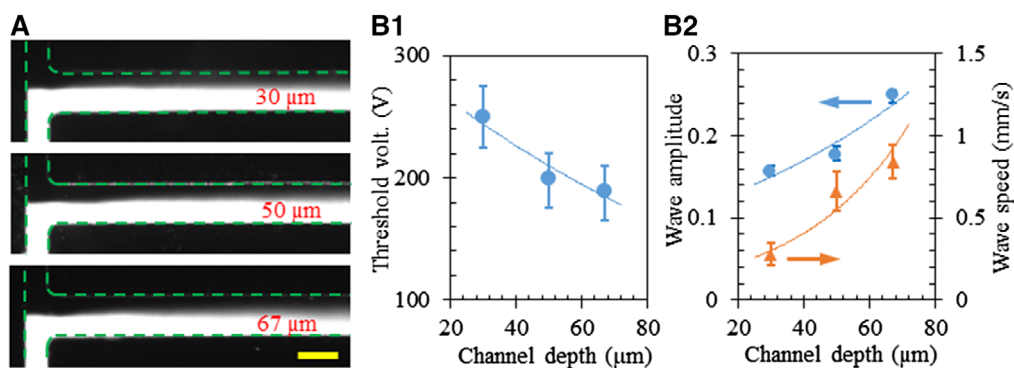


Figure 8. Effect of channel depth (labeled on the images) on the elastic instability in the EOF of 1 mM PB-based 200 ppm PAA solution: (A) shows the experimental images of the fluid interface at the T-junction under the threshold voltages; (B1) shows a graph for the measured threshold voltage; (B2) shows a graph for the measured wave amplitude (relative to the width of the main-branch) and speed under 250 V DC. The curves in (B1) and (B2) represent the trendlines that are fitted to the experimental data points (symbols). The dashed lines on the images highlight the channel walls, and the scale bar represents 200 μm.

because of the decreased fluid shear rate. We also measured the wave amplitude and speed of electro-elastic instabilities in the PAA solution of varying PB concentrations under a fixed DC voltage of 250 V (Figure 7B2). As expected from the reduced fluid elasticity and shear thinning effects, both wave parameters decrease when the PB concentration increases. Moreover, the measured wave frequency is found to decrease at a higher PB concentration (see Supporting Information Figure S-3) because of likely the same reasons as noted above.

3.2.3 Effect of channel dimensions

Figure 8 shows the effect of channel depth on the electro-elastic instability in 1 mM PB-based 200 ppm PAA solution. Similar flow patterns were observed in the T-shaped microchannels of 30, 50, and 67 μm deep, respectively (Fig. 8A). However, the measured threshold voltage shows a significant drop with the increase in channel depth. This trend is illustrated in Figure 8B1 and seems to be consistent with that of the threshold voltage for electrokinetic instabilities in Newtonian fluids with strong conductivity gradients [56]. We attribute such a phenomenon to the stabilizing effect of the top and bottom channel walls [57,58], which decreases in a deeper microchannel. Another factor that we think may also play a role is the relatively thinner EDL in a deeper microchannel, whereby the influence of the large stresses developed inside the EDL [38] should become less. We did not test the effect of channel width, but speculate that increasing it should also delay the onset of electro-elastic instabilities and hence increase the threshold voltage because of the similar reasons as stated above. Figure 8B2 shows the measured amplitude and speed of electro-elastic instability waves in the three depths of microchannels under the DC voltage of 250 V. Both wave parameters increase in a deeper channel because of the weakened wall stabilizing effect. However, the measured wave frequency is found to remain at roughly 1 Hz in all channels (see Supporting Information Figure S-4).

4 Concluding remarks

We have presented a systematic experimental study of the fluid rheological effects on the elastic instability in the EOF of various non-Newtonian fluids through T-shaped microchannels. It is found that the fluid shear thinning might be the primary cause for the observed electro-elastic instabilities because they occur only in the PAA and XG solutions with strong shear thinning effects. The fluid elasticity alone does not seem to be sufficient to draw any disturbances to the EOF because no instabilities are observed in the viscoelastic PVP, PEO or HA solution with a weak shear thinning effect. These observations seem to agree with our recently reported instabilities in the EOF of polymer solutions (other than the HA solution) through a constriction microchannel [36]. They are, however, inconsistent with the numerical predictions in the paper from Pimenta and Alves [38], who used an Oldroyd-B model to simulate the fluid elasticity effect alone on electro-elastic instabilities in cross-shaped microchannels. It is possibly because of the microstructural effects (e.g., polymer-wall interaction and electric effect on molecular structure of polymer, etc.) that occur in shear-thinning polymer solutions (e.g., the gelification under relatively low DC voltages [34, 38]) but are ignored in this work.

We have also studied the parametric effects on the electro-elastic instability in PB-based PAA solutions. It is found that the threshold voltage for the onset of instabilities decreases with the increase of polymer concentration because of the enhanced shear thinning effect and maybe the enhanced elasticity effect as well. However, increasing the buffer concentration causes a rise of the threshold voltage because the addition of salt reduces the fluid shear thinning and elasticity effects. The threshold voltage is found to also increase in a shallower microchannel mainly because of the strengthened wall stabilizing effect. Moreover, we have measured and analyzed the wave parameters, including amplitude, speed and frequency, for electro-elastic instabilities in both XG and PAA solutions under various working conditions. This work

provides the knowledge on how to better control the EOF of non-Newtonian fluids for various microfluidic applications such as mixing [59], DNA hybridization [60], and separation [61], etc. The former two applications favor elastic instabilities while the last one requires a suppression of any instabilities. Further studies, particularly theoretical or numerical simulations using for example, the Giesekus model [62], are needed to identify both the individual and the combined effects of fluid elasticity and shear thinning on electro-elastic instabilities.

This work was supported in part by China Scholarship Council (CSC) - Chinese Government Graduate Student Overseas Study Program (L.S.), University 111 Project of China under grant number B12019 (L.Y.), and NSF under grant number CBET-1704379 (X.X.).

The authors have declared no conflict of interest.

5 References

- [1] Li, D., *Electrokinetics in Microfluidics*, Elsevier Academic Press, Burlington, MA 2004.
- [2] Chang, H. C., Yeo, L. Y., *Electrokinetically Driven Microfluidics and Nanofluidics*, Cambridge University Press, New York 2010.
- [3] Whitesides, G. M., Stroock, A. D., *Phys. Today* 2001, 54, 42–48.
- [4] Zhao, C., Yang, C., *Microfluid. Nanofluid.* 2012, 13, 179–203.
- [5] Ghosal, S., *Electrophoresis* 2014, 25, 214–228.
- [6] Ghosal, S., *Annu. Rev. Fluid Mech.* 2006, 38, 309–338.
- [7] Stroock, A. D., Weck, M., Chiu, D. T., Huck, W. T. S., Kenis, P. J. A., Ismagilov, R. F., Whitesides, G. M., *Phys. Rev. Lett.* 2000, 84, 3314–3317.
- [8] Ghosh, U., Chakraborty, S., *Phys. Fluids* 2016, 28, 062007.
- [9] Schasfoort, R. B., Schlautmann, S., Hendrikse, J., van den Berg, A., *Science* 1999, 286, 942–945.
- [10] Lee, C. Y., Lee, G. B., Fu, L. M., Lee, K. H., Yang, R. J., *J. Micromech. Microeng.* 2004, 14, 1390–1398.
- [11] Zehavi, M., Boymelgreen, A., Yossifon, G., *Phys. Rev. Appl.* 2016, 5, 044013.
- [12] Prabhakaran, R. A., Zhou, Y., Zhao, C., Hu, G., Song, Y., Wang, J., Yang, C., Xuan, X., *Phys. Fluids* 2017, 29, 062001.
- [13] Cetin, B., Li, D., *Electrophoresis* 2008, 29, 994–1005.
- [14] Lapizco-Encinas, B. H., *Electrophoresis* 2019, 40, 358–375.
- [15] Nguyen, N. T., Wu, Z., *J. Micromech. Microeng.* 2005, 15, R1–R16.
- [16] Cai, G., Xue, L., Zhang, H., Lin, J., *Micromachines* 2017, 8, 274.
- [17] Chang, C. C., Yang, R. J., *Microfluid. Nanofluid.* 2007, 3, 501–525.
- [18] Lee, C. Y., Chang, C. L., Wang, Y. N., Fu, L. M., *Int. J. Mol. Sci.* 2011, 12, 3263–3287.
- [19] Lin, H., *Mech. Res. Comm.* 2009, 36, 33–38.
- [20] Lin, H., Storey, B. D., Oddy, M. H., Chen, C., Santiago, J. G., *Phys. Fluids* 2004, 16, 1922–1935.
- [21] Chen, C., Lin, H., Lele, S. K., Santiago, J. G., *J. Fluid Mech.* 2005, 524, 263–303.
- [22] Kang, K. H., Park, J., Kang, I. S., Huh, K. Y., *Int. J. Heat Mass Trans.* 2006, 49, 4577–4583.
- [23] Boy, D. A., Storey, B. D., *Phys. Rev. E* 2007, 76, 026304.
- [24] Lin, H., Storey, B. D., Santiago, J. G., *J. Fluid Mech.* 2008, 608, 43–70.
- [25] Luo, W. J., *Microfluid. Nanofluid.* 2009, 6, 189–202.
- [26] Li, Q., Delorme, Y., Frankel, S. H., *Microfluid. Nanofluid.* 2016, 20, 29.
- [27] Dubey, K., Gupta, A., Bahga, S. S., *Phys. Fluids* 2017, 29, 092007.
- [28] Navaneetham, G., Posner, J. D., *J. Fluid Mech.* 2009, 619, 331–365.
- [29] Song, L., Jagdale, P., Yu, L., Liu, Z., Zhang, C., Gao, R., Xuan, X., *Microfluid. Nanofluid.* 2018, 22, 134.
- [30] Posner, J. D., Perez, C. L., Santiago, J. G., *Proc. Natl. Acad. Sci. USA* 2012, 109, 14353–14356.
- [31] Wang, G., Yang, F., Zhao, W., *Lab Chip* 2014, 14, 1452–1458.
- [32] Zhao, C., Yang, C., *Adv. Colloid. Interf. Sci.* 2013, 201–202, 94–108.
- [33] D'Avino, G., Greco, F., Maffettone, P. L., *Annu. Rev. Fluid Mech.* 2017, 49, 341–360.
- [34] Bryce, R. M., Freeman, M. R., *Phys. Rev. E* 2010, 81, 036328.
- [35] Bryce, R. M., Freeman, M. R., *Lab Chip* 2010, 10, 1436–1441.
- [36] Ko, C. H., Li, D., Malekanfard, A., Wang, Y. N., Fu, L. M., Xuan, X., *Electrophoresis* 2019, 40, 1387–1394.
- [37] Afonso, A. M., Pinho, F. T., Alves, M. A., *J. Non-Newtonian Fluid Mech.* 2012, 179–180, 55–68.
- [38] Pimenta, F., Alves, M. A., *J. Non-Newtonian Fluid Mech.* 2018, 259, 61–77.
- [39] Song, L., Jagdale, P., Yu, L., Liu, Z., Li, D., Zhang, C., Xuan, X., *Phys. Fluids* 2019, 31, 082001.
- [40] Kumar, D. T., Zhou, Y., Brown, V., Lu, X., Kale, A., Yu, L., Xuan, X., *Microfluid. Nanofluid.* 2015, 19, 43.
- [41] Japper-Jaafar, A., Escudier, M. P., Poole, R. J., *J. Non-Newtonian Fluid Mech.* 2010, 165, 1357–1372.
- [42] Liu, C., Xue, C., Chen, X., Shan, L., Tian, Y., Hu, G., *Anal. Chem.* 2015, 87, 6041–6048.
- [43] Lim, H., Back, S. M., Hwang, M. H., Lee, D., Choi, H., Nam, J., *Micromachines* 2019, 10, 0462.
- [44] Rodd, L. E., Scott, T. P., Boger, D. V., Cooper-White, J. J., McKinley, G. H., *J. Non-Newtonian Fluid Mech.* 2005, 129, 1–22.
- [45] Poole, R. J., Escudier, M. P., *J. Non-Newtonian Fluid Mech.* 2004, 117, 25–46.
- [46] Lindner, A., Bonn, D., Meunier, J., *Phys. Fluids* 2000, 12, 256–261.
- [47] Zhang, J., Yan, S., Yuan, D., Alici, G., Nguyen, N. T., Warkiani, M. E., Li, W., *Lab Chip* 2016, 16, 10–34.

- [48] Stoecklein, D., Di Carlo, D., *Anal. Chem.* 2019, *91*, 296–314.
- [49] Leshansky, A. M., Bransky, A., Korin, N., Dinnar, U., *Phys. Rev. Lett.* 2007, *98*, 234501.
- [50] Aytouna, M., Paredes, J., Shahidzadeh-Bonn, N., Moulinet, S., Wagner, C., Amarouchene, Y., Eggers, J., Bonn, D., *Phys. Rev. Lett.* 2013, *110*, 034501.
- [51] Sousa, P. C., Pinho, F. T., Oliveira, M. S. N., Alves, M. A., *Soft Matter* 2015, *11*, 8856–8862.
- [52] Tirtaatmadja, V., Mckinley, G. H., Cooper-White, J. J., *Phys. Fluids* 2006, *18*, 043101.
- [53] Ballesta, P., Alves, M. A., *Phys. Rev. Fluids* 2017, *2*, 053301.
- [54] Campo-Deaño, L., Galindo-Rosales, F. J., Pinho, F. T., Alves, M. A., Oliveira, M. S. N., *J. Non-Newtonian Fluid Mech.* 2011, *166*, 1286–1296.
- [55] Kirby, B. J., Hasselbrink, E. F., *Electrophoresis* 2004, *25*, 187–202.
- [56] Song, L., Yu, L., Zhou, Y., Antao, A. R., Prabhakaran, R. A., Xuan, X., *Sci. Rep.* 2017, *7*, 46510.
- [57] Storey, B. D., Tilley, B. S., Lin, H., Santiago, J. G., *Phys. Fluids* 2005, *17*, 018103.
- [58] Oliveira, M. S. N., Pinho, F. T., Alves, M. A., *J. Fluid Mech.* 2012, *711*, 171–191.
- [59] Kunti, G., Bhattacharya, A., Chakraborty, S., *J. Non-Newtonian Fluid Mech.* 2017, *247*, 123–131.
- [60] Das, S., Das, T., Chakraborty, S., *Sens. Actuators B* 2006, *114*, 957–963.
- [61] Das, S., Chakraborty, S., *Electrophoresis* 2008, *29*, 1115–1124.
- [62] Bird, R. B., *Annu. Rev. Fluid Mech.* 1995, *27*, 169–193.